



PCCP

Preparation of Visible Light-driven g-C₃N₄@ZnO Hybrid Photocatalyst via Mechanochemistry

Journal:	<i>Physical Chemistry Chemical Physics</i>
Manuscript ID:	CP-ART-05-2014-002061.R1
Article Type:	Paper
Date Submitted by the Author:	21-Jun-2014
Complete List of Authors:	Chow, Jianwei; Institution of Energy and Feul, Xinxiang University; Tsinghua University, Chemistry Zhang, Mo; Beijing Normal University, Departement of Chemistry Zhu, Yongfa; Tsinghua University,

SCHOLARONE™
Manuscripts

Cite this: DOI: 10.1039/c0xx00000x

www.rsc.org/xxxxxx

PAPER

Preparation of Visible Light-driven g-C₃N₄@ZnO Hybrid Photocatalyst via Mechanochemistry

Jianwei Zhou^{a, b}, Mo Zhang^b, and Yongfa Zhu^{b*}*Received (in XXX, XXX) Xth XXXXXXXXX 20XX, Accepted Xth XXXXXXXXX 20XX*

DOI: 10.1039/b000000x

C₃N₄@ZnO hybrid materials with visible light photocatalytic performance have been prepared by facile mechanical milling. The dispersion of conjugated molecule g-C₃N₄ on the surface of ZnO was improved during mechanical milling. And the multilayer hybrid structure of g-C₃N₄@ZnO materials with remarkable visible light photocatalytic activity was formed by ball milling. The photocatalytic activity and photocurrent intensity of g-C₃N₄@ZnO under visible light irradiation was 3.0 and 2.0 times higher than pure C₃N₄ respectively. The great enhancement of visible light response originates from the increase of separation and immigration efficiency of photogenerated electron-hole pairs. Furthermore, a synergistic photocatalysis mechanism between ZnO and g-C₃N₄ was proposed. The enhanced visible photocatalytic properties originate from the injection of excited electrons from the LUMO of C₃N₄ to the CB of ZnO. However, the photocatalytic activity of the photocatalyst is much lower than that of ZnO under UV light, which is caused by the lattice defect of ZnO formed during milling.

Introduction

Photocatalysis technology is widely used for the degradation of organic pollutants. To develop novel materials with nontoxicity, low cost, and long-term stability has attracted great attention. Zinc oxide (ZnO), an important kind of semiconductor with a wide band gap of 3.37 eV, deep oxidation capability and low cost, is proved to exhibit higher photocatalytic activity than TiO₂ in some conditions¹⁻⁴. However, the photocorrosion of ZnO materials was found to be severe during the reaction by the action of the photogenerated holes, which may affect the stability and photocatalytic activity of ZnO⁵⁻¹⁰. In addition, its application is also limited by the low quantum efficiency and incompetent visible light harvesting. There have been many attempts to enhance its photocatalytic performance, such as doping^{11, 12}, depositing metals¹³⁻¹⁵ and coupling with semiconductors¹⁶⁻²⁰. With conjugated π system, graphitic carbon nitride (g-C₃N₄) exhibits high chemical and thermal stability, versatility in mechanical, electronic and optical properties due to the outstanding separation and migration efficiency of photogenerated electron-hole pairs²¹⁻²⁵. It has been reported that organic surface coating of ZnO could enhance the separation of photoinduced carriers and protect ZnO from photo-corrosion^{26,27}. Although there have been many attempts to prepare hybrid photocatalysts in the liquid phase, the solid phase synthesis is rarely reported²⁸. Herein, g-C₃N₄@ZnO hybrid materials with visible light photocatalytic performance have been prepared by facile mechanical milling. The visible light photocatalytic activity is significantly improved by the expanded light response range and the photocorrosion is effectively inhibited. The mechanism of the enhancement of photocatalytic activity is also discussed.

Experimental

The morphologies and structures of the samples were examined with transmission electron microscopy (TEM) by Hitachi HT-7700 TEM and JEM 1010 HRTEM operated at an accelerating voltage of 100 kV and 200 kV, respectively. UV-Vis diffuse reflectance spectroscopy (DRS) was carried out on a Hitachi U-3010 UV-vis spectrophotometer. BaSO₄ was the reference sample. The Brunauer-Emmett-Teller (BET) surface area was measured by ASAP 2010 V5.02H. The crystallinity of the as-prepared sample was characterized by X-ray diffraction (XRD) on Bruker D8-advance diffractometer using Cu-K α radiation ($\lambda=1.5418$ Å). The photocurrents were measured on an electrochemical system (CHI 660B, China). Visible light was obtained from a 500 W xenon lamp (Institute for Electric Light Sources, Beijing) with a 420 nm cutoff filter.

The g-C₃N₄ was synthesized by directly heating melamine. In a typical run, 5 g melamine powder was put into an alumina crucible and heated in a muffle furnace at 530 °C for 4 h with a heating rate of 5 °C·min⁻¹. After cooling to room temperature, the product was collected and ground into powder. The preparation of C₃N₄@ZnO photocatalyst was carried out in a ball miller (XQM-0.4, made in Changsha, China). The procedure of preparation is as follows: ZnO powder and agate ball are mixed in the agate ball milling tank with a ratio of 1:10, and then a certain amount of C₃N₄ is added. After being milled for a certain time with different speed, the final samples are used for the determination of photocatalytic activity and characterization.

The photocatalytic activities were evaluated by the decomposition of methylene blue (MB). Visible irradiation was obtained from a 500 W Xe lamp (Institute for Electric Light

Sources, Beijing) with a 420 nm cutoff filter, and the average visible light intensity was $35 \text{ mW}\cdot\text{cm}^{-2}$. The UV irradiation was obtained from a 300 W Hg lamp with a 365 nm cutoff filter. The average intensity was $1.2 \text{ mW}\cdot\text{cm}^{-2}$. The concentration of MB was analyzed by recording the absorbance at the characteristic band of 664 nm using a Hitachi U-3010 UV-Vis spectrophotometer. To investigate the degradation mechanism, radical trapping experiments were performed under visible and UV light irradiation. The reaction condition was that photodegradation of MB with the addition of $1 \text{ mmol}\cdot\text{L}^{-1}$ hydroxyl radical scavenger (tBuOH) and $1 \text{ mmol}\cdot\text{L}^{-1}$ hole scavenger (EDTA-2Na).

To investigate the transition of photogenerated electrons of $\text{g-C}_3\text{N}_4$, a standard three-electrode cell with a working electrode (as-prepared photocatalyst), a platinum wire as counter electrode, and a standard calomel electrode (SCE) as reference electrode were used in the photoelectric studies. $0.1 \text{ M Na}_2\text{SO}_4$ was used as the electrolyte solution. Potentials were given with reference to the SCE. The photoresponses of the photocatalysts as light on and off were measured at 0.0 V . The working electrodes were prepared as follows: 10 mg of the as-prepared photocatalyst was suspended in 1 mL ethanol to produce a slurry, which was then dip-coated onto a $2 \text{ cm} \times 4 \text{ cm}$ indium tin oxide (ITO) glass electrode. Electrodes were exposed to air atmosphere for 12 h to eliminate water and subsequently calcined at $150 \text{ }^\circ\text{C}$ for 5 hours .

Results and discussion

Formation of hybrid catalysts *via* mechanical milling

Table 1 The specific surface area of the sample at different milling speed

Samples	ZnO		3%- C_3N_4 @ZnO		
	Without milled	350 rpm	250 rpm	300 rpm	350 rpm
$S_{\text{BET}}(\text{m}^2/\text{g})$	10.3	13.0	12.3	12.1	12.5

As shown in Table 1 and S1, the specific surface area (S_{BET}), pore volume (V_p), and average pore diameter of pure ZnO increases after ball milling, indicating the smaller particle size of milled ZnO. The values of S_{BET} , V_p and average pore diameter of 3%- C_3N_4 @ZnO do not changed obviously with the increase of milling speed. However, the values of S_{BET} , V_p and average pore diameter of C_3N_4 @ZnO are decreased with the increase of milling speed, which may be attributed to the mechanical and chemical interaction between C_3N_4 and ZnO and the dispersion state of C_3N_4 .

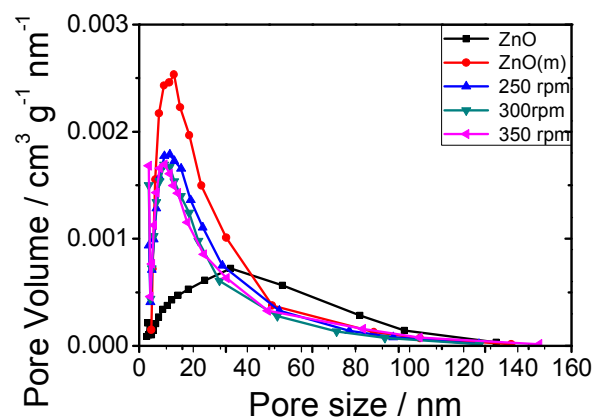


Figure 1 The pore size distribution curves of samples

Figure 1 shows the pore size distribution curves of samples determined from the adsorption branch of the isotherms. The hybrid photocatalysts prepared by ball milling show more apparent pore distribution than pure ZnO. Typical nanopores appear as broad peak at $5\text{--}40 \text{ nm}$ for hybrid photocatalyst, and the peak point is about 10 nm . While the changes of pore size distributions of hybrid catalyst prepared at different milling speed are less obvious, which may be attributed to the mechanical and chemical interaction between C_3N_4 and ZnO and the dispersion state of C_3N_4 .

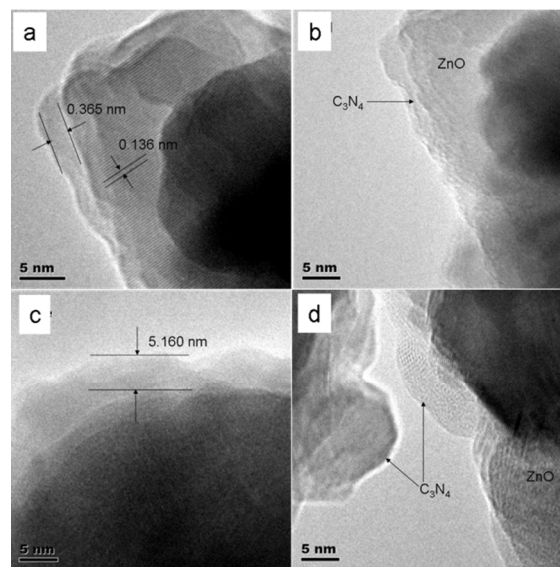


Figure 2 High-resolution TEM images of 3%- C_3N_4 @ZnO (a) (b), 7%- C_3N_4 @ZnO (c) (d)

As can be seen from the HRTEM images (Fig 2), the d-spacing of ZnO is 0.136 nm , corresponding to the (201) interplanar spacing. The High-resolution TEM images of 3%- C_3N_4 @ZnO show that the ZnO particles are surrounded by C_3N_4 layers, and the overall thickness of the C_3N_4 shell is about 0.365 nm , which is identical to the thickness of a monolayer of C_3N_4 . Therefore, it can be estimated that the ZnO particles are surrounded by C_3N_4 monolayers. As shown in images of 7%- C_3N_4 @ZnO, the thickness of C_3N_4 layers around ZnO particles is about 5 nm , indicating the multilayer loading of C_3N_4 .

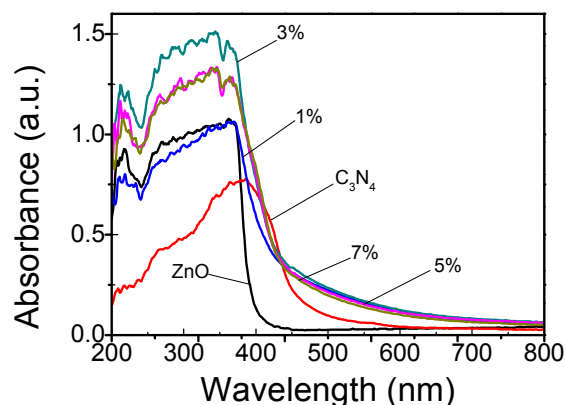


Figure 3 UV-vis diffuse reflectance spectra of C_3N_4 , ZnO and $C_3N_4@ZnO$

The optical properties of the $C_3N_4@ZnO$ materials were probed with UV-vis diffuse reflectance spectroscopy, shown in Figure 3. The absorption edge of $C_3N_4@ZnO$ samples expanded to the visible light region due to the presence of C_3N_4 on the ZnO surface, indicating the effective surface hybridization of ZnO by mechanical milling. The absorption of visible light was originated from C_3N_4 on the surface of the $C_3N_4@ZnO$ materials.

10 Formation of hybrid catalysts *via* mechanical milling

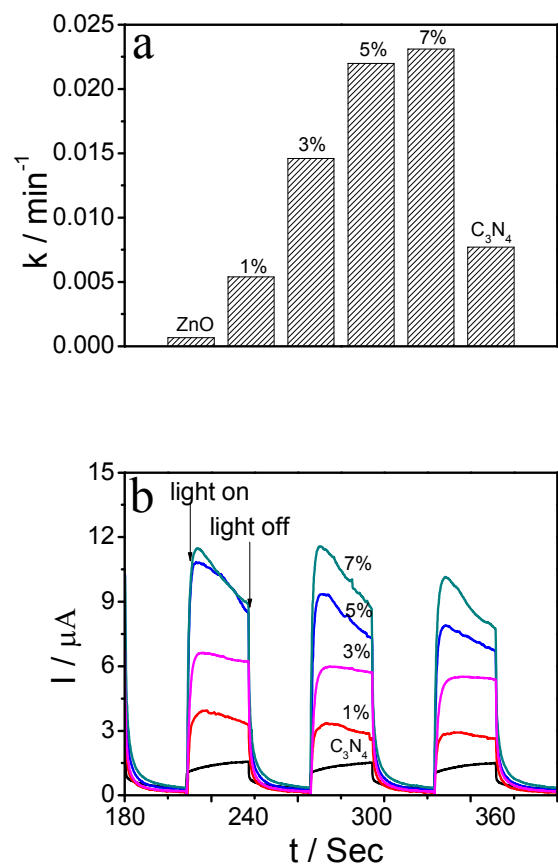
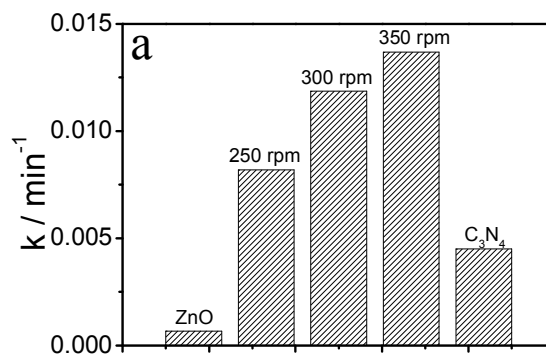


Figure 4 Visible light photocatalytic degradation of MB (1×10^{-5} mol/L) by $g-C_3N_4@ZnO$ with various weight content of C_3N_4 (1%, 3%, 5%, and 7%) under 500 W Xe lamp, 420 nm cutoff filter (a) Photocurrent

responses of samples at different weight content of C_3N_4 (1%, 3% and 5%), under 500 W Xe lamp, 420 nm cutoff filter (b)

As shown in Fig 4a, $C_3N_4@ZnO$ materials show higher photocatalytic activity under visible light. And the degradation rate of MB by them is increased with the increasing amount of C_3N_4 loading. The degradation rate increased to about 3 times of pure C_3N_4 when the amount of C_3N_4 loading was increased from 1% to 7%. The result implies that the separation and migration efficiency of photogenerated electron-hole pairs was improved by the surface hybridization of C_3N_4 , which resulted in the enhancement of photocatalytic activity. The photocatalytic activity under visible light mainly generated from C_3N_4 . The migration efficiency of photo induced carriers was enhanced by the conjugated π bond. The ZnO material, as the electron acceptor, can further increase the separation efficiency of photogenerated electron-hole pairs.

Figure 4b shows that the photocurrent of hybridized catalysts under visible light irradiation was in order of 5%- $C_3N_4@ZnO$ > 3%- $C_3N_4@ZnO$ > 1%- $C_3N_4@ZnO$ > C_3N_4 , which coincides with that of the photocatalytic activity under visible light. The photocurrent under visible light was mainly originated from C_3N_4 and was determined by the separation efficiency of photogenerated carriers of C_3N_4 materials. Therefore, the photocurrent was enhanced with the increasing amount of C_3N_4 loading and was larger than that of pure C_3N_4 due to the improved separation efficiency of photogenerated carriers, thanks to the ZnO as the electron acceptor. Under visible light irradiation, the photocurrent of 5%- $C_3N_4@ZnO$ was about 8 times as high as that of C_3N_4 . The photocurrent reflects the separation efficiency of photogenerated carriers, hence the hybridization of C_3N_4 can effectively improve the separation efficiency of photogenerated electron-hole pairs.



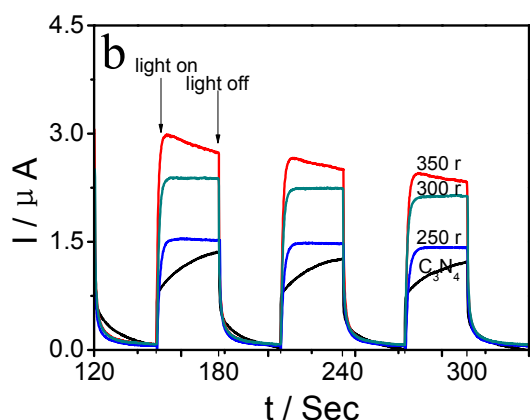


Figure 5a Photocatalytic degradation of MB ($C_0=1\times 10^{-5}$ mol/L) by $g\text{-C}_3\text{N}_4@ZnO$ with various ball milling rate ($r = 250$ rpm, 300 rpm and 350 rpm) under 500 W Xe lamp irradiation, 420 nm cutoff filter (a) Transient photocurrent responses of different ball milling rate under visible light (500 W Xe lamp irradiation, 420 nm cutoff filter) (b)

As shown in Fig 5a, the photocatalytic activity of hybridized catalysts under visible light was enhanced with the increased milling speed and fixed milling time. The reaction rate of the catalyst produced by milling speed of 350 rpm was about 3 times as high as pure C_3N_4 . Fig.5b shows that the photocurrent under visible light irradiation was in order of $I_{350r} > I_{300r} > I_{250r} > I_{C_3N_4}$. The result indicates that the photocurrent of $C_3N_4@ZnO$ materials was increased remarkably with the increase of milling speed. The photocurrent of hybridized catalyst produced by milling speed of 350 rpm was about 2 times as high as pure C_3N_4 . The enhancement of photocurrent implied that there were interactions between C_3N_4 and ZnO. The separation efficiency of photogenerated electron-hole pair was increased by the modification of C_3N_4 molecules, and thereby the photocurrent response was significantly improved as well.

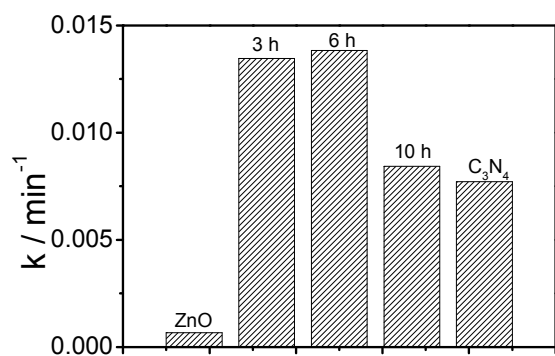


Figure 6 Effects of ball milling time on the photocatalytic activities of $g\text{-C}_3\text{N}_4@ZnO$ under visible light

The effect of ball milling time on the photocatalytic activity of $g\text{-C}_3\text{N}_4@ZnO$ hybrid photocatalyst is shown in Fig.6. The optimum milling time is 6 h, and the reaction rate of 6h is about 1.2 times as that of 10 h. The result is mainly caused by the increased

activity sites and crystal lattice distortion of ZnO in the process of ball milling.

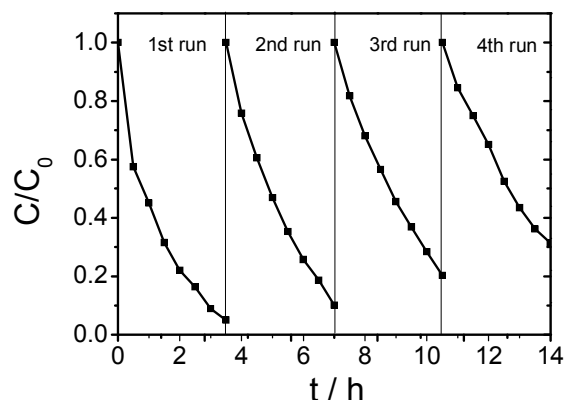
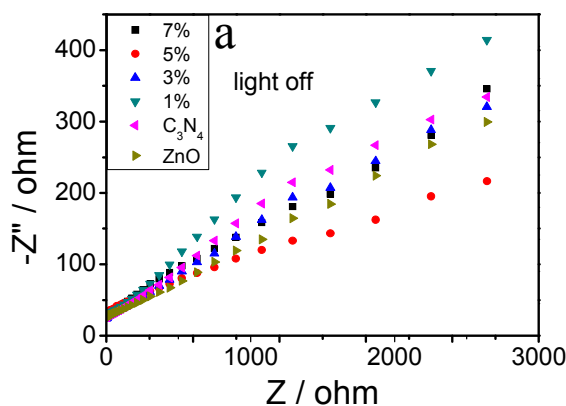


Figure 7 The stability of $g\text{-C}_3\text{N}_4@ZnO$ ($C_{MB}=1\times 10^{-5}$ mol/L, Cat. 50 mg/100 mL, $\lambda > 420$ nm)

The stability is of great significant for photocatalysts in practical application. The photoactivity of 3%- $C_3N_4@ZnO$ was recycling tested under visible light. It is shown in Fig.7 that the photocatalyst exhibits stable photocatalytic activity for decomposing MB after four cycling. The small decline in activity is mainly due to the loss of catalyst during the experiment process. Therefore, it is determined that the MB degradation abilities of $g\text{-C}_3\text{N}_4@ZnO$ are not decreased and the photocatalytic activities of them are stable, indicating the strong hybridization effect between C_3N_4 and ZnO.

4.5 Mechanism of enhanced activity by mechanical milling



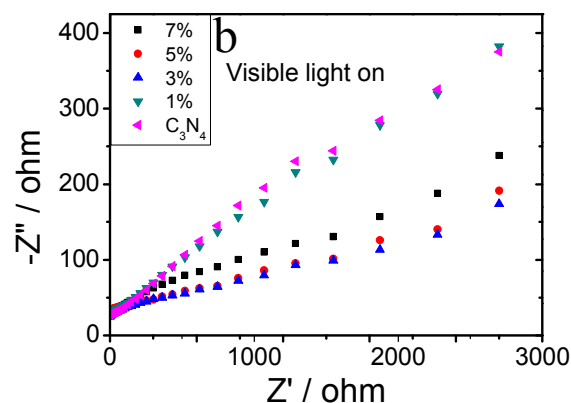


Figure 8 Electrochemical impedance spectroscopy (EIS) Nyquist plot of C_3N_4 and $g-C_3N_4@ZnO$

As shown in Fig.8, charge transfer on the surface of electrode is determined to be the rate determining step according to the arc on the EIS Nyquist plot of all the samples. The arc radius on the EIS Nyquist plot of all $ITO/C_3N_4@ZnO$ electrodes was smaller than that of the ITO/C_3N_4 electrode under visible light, which meant a more effective separation of photogenerated electron-hole pairs and faster interfacial charge transfer had occurred. The result is consistent with that of photocurrent.

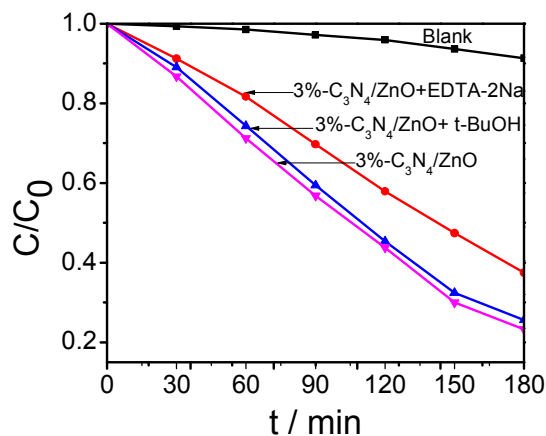


Figure 9 The capture experiment of active species of $3\%-C_3N_4@ZnO$ under visible light

The radicals trapping experiments under visible light are employed to investigate the photocatalysis mechanism of $g-C_3N_4@ZnO$ materials. The water pollutant can be degraded by the radicals (OH^\bullet , $O_2^{\bullet-}$ and holes) generated during the photocatalysis reaction. Figure 9 demonstrates that photocatalytic activity of $g-C_3N_4@ZnO$ was remarkably reduced by addition of tert-Butyl alcohol as hydroxyl radical scavenger, which implies that holes and $O_2^{\bullet-}$ radicals are the main oxidative species in the reaction process of $g-C_3N_4@ZnO$.

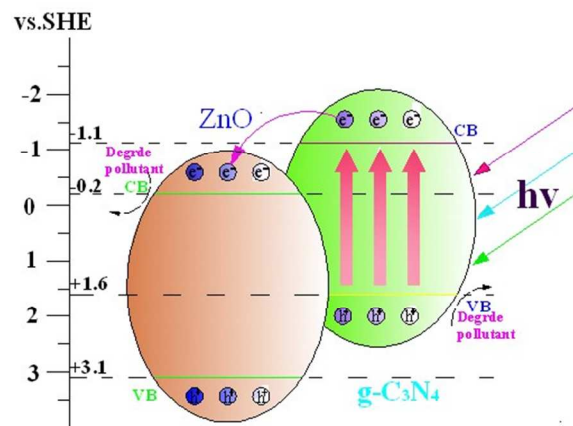
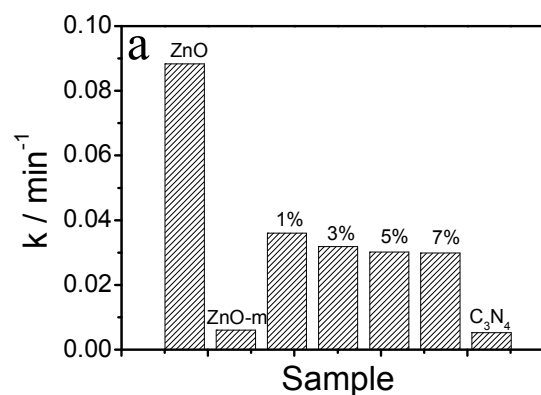


Figure 10 Schematic illustration of electron-hole separation and transport and photocatalytic activity of the $g-C_3N_4@ZnO$ photocatalyst under visible light irradiation.

On the basis of the above analysis, it can be concluded that the photocatalytic activity of the $g-C_3N_4@ZnO$ hybrid under visible light may be mainly attributed to chemical effect between C_3N_4 and ZnO . The possible mechanism is shown in Fig 10. It is well known that ZnO itself cannot be excited by visible light. The C_3N_4 can be excited by visible light and photogenerated electrons were generated on LUMO. The LUMO position of C_3N_4 (-1.1 eV) is higher than that of the conduction band (CB) of ZnO (-0.2 eV), so the photogenerated electrons on LUMO of C_3N_4 can be easily injected into the CB of ZnO and subsequently transfer to the surface of the $C_3N_4@ZnO$ hybrid to react with water and oxygen. This reaction yielded hydroxyl and superoxide radicals that were able to oxidize the pollutants because of their high oxidative capacity, producing visible photocatalytic activity.

Influence of mechanical milling on UV photoactivity



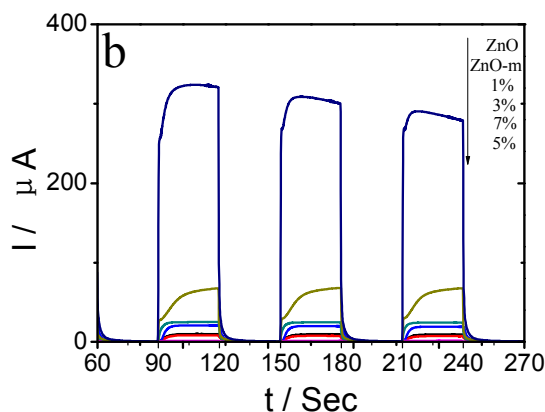


Figure 11 Photocatalytic activity of g-C₃N₄@ZnO with different contents of C₃N₄ (1%, 3%, 5% and 7%) under UV light (300 W high pressure mercury lamp, 365 nm) (a) Photocurrent responses of different content of C₃N₄ (1%, 3%, 5% and 7%) under UV light (15 W mercury lamp, 254 nm wavelength, ZnO (m)-milled ZnO) (b)

As shown in Fig 11a, the photocatalytic activity of g-C₃N₄@ZnO materials under UV irradiation decreased with the addition of C₃N₄ loading. The photocatalytic activity of hybridized catalysts with low content of C₃N₄ was slightly higher, but was much lower than pure ZnO. The reduced photocatalytic activity under UV was mainly caused by the generation of defects during the mechanical milling process.

Fig 11b shows that the photocurrent under UV irradiation was in order of pure ZnO > 1%-C₃N₄@ZnO > 3%-C₃N₄@ZnO > 5%-C₃N₄@ZnO > 7%-C₃N₄@ZnO > pure C₃N₄ and presented the similar change trend to that of photocatalytic activity under UV irradiation. Compared with pure ZnO, the photocurrent of milled pure ZnO was greatly reduced. On the one hand, the reduction of photocurrent for hybridized catalysts was due to the decrease of UV absorption by surface hybridization of C₃N₄. On the other hand, the defects on the surface of milled ZnO became the recombination center of photogenerated carriers, which decreased the photocurrent as well.

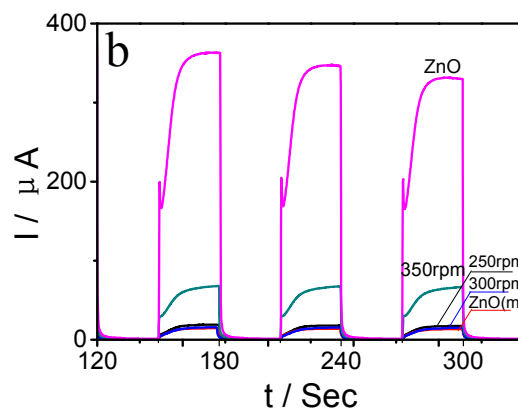
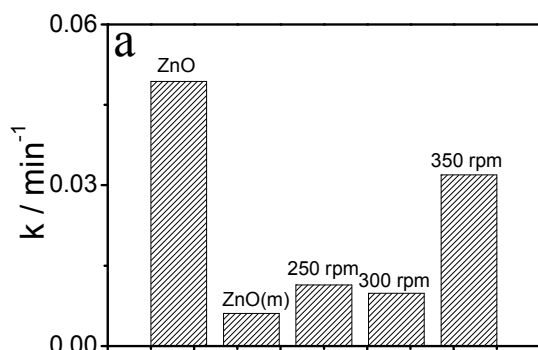


Figure 12 Effects of ball milling rate on the photocatalytic activity under UV light irradiation (Under 300 W Hg lamp with 365 nm) (a) Transient photocurrent responses of different ball milling rate under UV light (15 W mercury lamp, 254 nm) (b)

Fig 12a shows the photocatalytic activity of catalysts produced by different milling speed. The catalyst produced by milling speed of 350 rpm exhibits the maximal activity in hybridized materials, but the activity is still lower than pure ZnO. To investigate the cause of decreased activity under UV light, the pure ZnO was milled using the same method. The photocatalytic activity of milled ZnO was decreased notably, which may be caused by the strain of the crystal structure and increasing defects on the surface of ZnO. The speculation was proved by photocurrent of catalysts produced by different milling speed (Fig 12b).

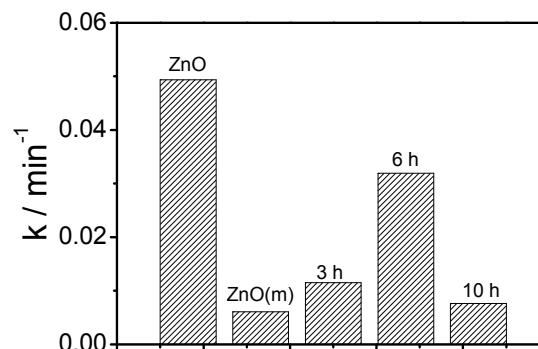


Figure 13 The influence of different ball milling time on activity under UV light

The UV activity is drastically decreased via mechanochemical method between C₃N₄ and ZnO hybridization, compared with pure ZnO without ball milling (Fig 13). The reason is that with the increased ball milling time, the crystal lattice distortion of ZnO and many defects may be produced in milling process, indicating the decreased separation efficiency of photo-excited charge carriers compared with pure ZnO.

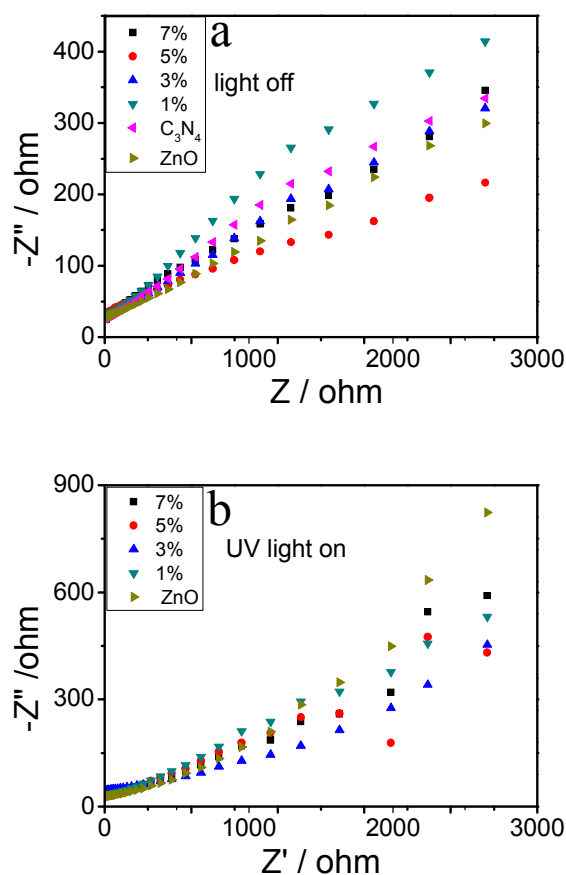


Figure 14 Electrochemical impedance spectroscopy (EIS) Nyquist plot of ZnO, C₃N₄ and g-C₃N₄@ZnO

As shown in Fig 14, charge transfer on the surface of electrode is determined to be the rate determining step according to the arc on the EIS Nyquist plot of all the samples. The arc radius on the EIS Nyquist plot of all ITO/C₃N₄@ZnO electrodes was smaller than that of the ITO/ZnO electrode under UV light, which is mainly because that the carrier concentration and the reaction rate were increased and the interfacial resistance was decreased under light irradiation. The result is consistent with that of photocurrent. The reduced photocatalytic activity under UV of g-C₃N₄@ZnO could probably be attributed to the formation of defects in the particles during the ball milling process. In the process of ball milling, the crystal lattice of ZnO undergoes severe plastic deformation, producing stresses and strains. Crystal lattice distortion of ZnO is caused and at the same time many defects inside ZnO particles are formed in the ball milling process. The defects became the recombination center of photogenerated carriers and the UV photocatalytic activity was decreased by that.

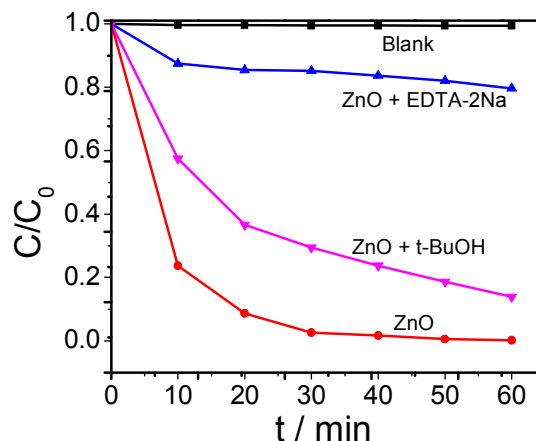


Figure 15 The capture experiment of active species of ZnO under UV light,

The radicals trapping experiments under UV light are employed to investigate the photocatalysis mechanism of g-C₃N₄@ZnO materials. As shown in Fig.15, the photocatalytic activity was somewhat reduced after adding tert-butyl alcohol as hydroxyl radical scavenger and was significantly inhibited after adding EDTA-2Na as hole radical scavenger, indicating that holes and OH• radicals are the main oxidative species on ZnO.

Conclusions

g-C₃N₄@ZnO hybrids visible light driven photocatalysts are prepared via mechanical milling. The hybrid photocatalysts showed obviously superior photocatalytic stability for the photodegradation of methylene blue. The visible light photocatalytic activity of g-C₃N₄@ZnO was 3.0 times as that of pure C₃N₄ sample due to the strong interaction between C₃N₄ and ZnO. The superior photocatalytic activity of the hybrid is mainly originated from the transition of photogenerated electrons on LUMO of C₃N₄ and the CB of ZnO. This simple mechanical milling method could be used as a universal pathway to improve the activity of photocatalyst and applied in the environmental remediation.

Acknowledges

This work was partly supported by National Basic Research Program of China (973 Program) (2013CB632403), National High Technology Research and Development Program of China (2012AA062701) and Chinese National Science Foundation (20925725 and 21373121)

Notes and references

- ^a Institute of energy and fuel, Xinxiang University, Xinxiang, China 453003, jwchow@163.com
^b Department of Chemistry, Tsinghua University, Beijing, China 100084, zhuyf@tsinghua.edu.cn
 † Electronic Supplementary Information (ESI) available: [TEM images, FT-IR spectra, XRD patterns, Raman spectra and fluorescence emission spectra of g-C₃N₄ and g-C₃N₄@ZnO are available in the supplementary information]. See DOI: 10.1039/b000000x/

- 1 A. A. Khodja, T. Sehili, J. F. Pilichowski, P. Boule, *J. Photo. Photobio. A*, 2001, **141**, 231-239.
- 2 B. Q. Cao, W. P., *J. Phys. Chem. C*, 2008, **112**, 680-685.
- 3 Y. M. Cristina, J. Rodrouez, J. Freer, N. Durán, H. Mansilla, *Chemosphere*, 2000, **41**, 1193-1197.
- 4 E. A. Meulenkamp, *J. Phys. Chem. B*, 1998, **102**, 7764-7769.
- 5 P. Spathis, I. Poullos, *Corros. Sci.*, 1995, **37**, 673-680.
- 6 A. van Dijken, A. H. Janssen, M. H. P. Smitsmans, D. Vanmaekelbergh, A. Meijerink., *Chem. Mater.* 1998, **10**, 3513-3522.
- 10 7 J. C. Wang, P. Liu, S. M. Wang, W. Han, X. X. Wang, X. Z. Fu, *J. Mol. Catal. A Chem.*, 2007, **273**, 21-25.
- 8 P. E. de Jongh, E. A. Meulenkamp, D. Vanmaekelbergh, J. J. Kelly, *J. Phys. Chem. B*, 2000, **104**, 7686-7693.
- 15 9 N. Daneshvar, D. Salari, A. R. Khataee, *J. Photoch. Photo. A*, 2004, **162**, 317-322.
- 10 X. Q. Qiu, L. P. Li, J. Zheng, J. J. Liu, X. F. Sun, G. S. Li, *J. Phys. Chem. C*, 2008, **112**, 12242-12248.
- 11 X. Q. Qiu, G. S. Li, X. F. Sun, L. P. Li, X. Z. Fu, *Nanotechnology*, 2008, **19**, 5703-5708.
- 20 12 J. Bandara, K. Tennakone, P. P. B., *Chemosphere*, 2002, **49**, 439-445.
- 13 L. Q. Jing, B. Q. Wang, B. F. Xin, S. D. Li, K. Y. Shi, W. M. Cai, H. G. Fu., *J. Solid State Chem.*, 2004, **177**, 4221-4227.
- 25 14 A. Stroyuk, V. V. Shvalagin, S. Y. Kuchmii, *Theor. Exp. Chem.* 2004, **40**, 98-104.
- 15 M. L. Zhang, T. C. An, X. H. Hu, C. Wang, G. Y. Sheng, J. M. Fu, *Appl. Catal. A- Gen.*, 2004, **260**, 215-222.
- 16 R. S. Mane, W. J. Lee, H. M. Pathan, S. H. Han, *J. Phys. Chem. B*, 2005, **109**, 24254-24259.
- 30 17 X. G. Chen, Y. Q. He, Q. Zhang, L. J. Li, D. H. Hu, T. Yin, *J. mater. sci.* 2010, **45**, 953-960.
- 18 R. Comparelli, E. Fanizza, M. L. Curri, P. D. Cozzoli, G. Mascolo, A. Agostiano, *Appl. Catal. A*, 2005, **60**, 1-11.
- 35 19 Y. Wang, R. Shi, J. Lin, Y. Zhu, *Energy Environ. Sci.*, 2011, **4**, 2922-2929.
- 20 G. Yu, J. Gao, J. C. Hummelen, F. Wudl, A. J. Heeger, *Science*, 1995, **270**, 1789-1791.
- 21 J. M. Hu, W. F. Cheng, S. P. Huang, D. S. Wu, Z. Xie, *Appl. Phys. Lett.*, 2006, **89**, 261117-261119.
- 40 22 Y. Wang, X. Bai, C. Pan, J. He, Y. Zhu, *J. Mater. Chem.* 2012, **22**, 11568-11573.
- 23 C. Pan, J. Xu, Y. Wang, D. Li, Y. Zhu, *Adv. Func. Mater.* 2012, **22**, 1518-1524.
- 45 24 X. Bai, L. Wang, R. Zong, Y. Zhu, *J. Phys. Chem. C*, 2013, **117**, 9952-9961.
- 25 H. B. Fu, T. G. Xu, S. B. Zhu, Y. F. Zhu, *Environ. Sci. Technol.* 2008, **42**, 8064-8069.
- 26 H. Zhang, R. L. Zong, Y. F. Zhu, *J. Phys. Chem. C.*, 2009, **113**, 4605-4611.
- 50 27 L. W. Zhang, H. Y. Cheng, R. L. Zong, Y. F. Zhu, *J. Phys. Chem. C.*, 2009, **113**, 2368-2374.
- 28 S. C. Yan, S. B. Lv, Z. S. Li, Z. G. Zou, *Dalton Trans.*, 2010, **39**, 1488-1491.